Synergistic Enhancement of CO_2 Biomethanation by Fe/Co/Ni-Loaded Biochar from Cattle Manure

Xin Cui, Jiaye Li, and Xin Li *

Carbon dioxide biomethanation offers a promising route for energy storage *via* biological conversion of renewable surplus electricity and CO_2 into methane. To improve the gas production efficiency and instability, bioaugmentation strategies are commonly employed by using biochar and trace elements individually. However, their coupled effect remains underexplored. In this study, the CM400 (biochar produced from cattle manure under 400 °C) showed superior performance in cumulative methane yield (138 mL·gVS^{-1}). Response surface optimization identified an optimal trace element combination (Fe: 15.1 mg·L^{-1}, Co: 1.5 mg·L^{-1}, Ni: 0.6 mg·L^{-1}), increasing methane yield by 12.9%. Subsequently, a novel modified biochar (CM400 pre-soaked in the optimal Fe/Co/Ni solution and pyrolyzed) was synthesized and significantly enhanced the volumetric methane production (VMP) by 19.8%. Experimentally, it enhanced the removal of total solids (TS), volatile solids (VS), and total chemical oxygen demand (TCOD) by 21.1%, 20.9%, and 3.4%, respectively, while strengthening pH buffering and preventing volatile fatty acid (VFA) accumulation. The modified biochar enriched electroactive bacteria (*e.g.*, *Synergistota*, *Chloroflexota*) and key methanogens (*Methanothrix*). Collectively, these physiological and compositional changes are consistent with improved syntrophic metabolism and suggest the possible involvement of direct interspecies electron transfer.

DOI: 10.15376/biores.21.4.10070-10097

Keywords: CO_2 biomethanation; Bioaugmentation; Biochar; Trace element

*Contact information: College of Engineering, China Agricultural University, Beijing 100083, China; *Corresponding author: lxin@cau.edu.cn*

INTRODUCTION

In a multi-energy distributed energy system, surplus electricity generated from photovoltaic and wind power systems is widely used to produce hydrogen through water electrolysis for efficient utilization of renewable energy. However, the high costs associated with hydrogen storage and long-distance pipeline transportation, coupled with the underdeveloped end-user hydrogen utilization infrastructure, limit the downstream development of the hydrogen industry (Han *et al.* 2025a). Meanwhile, the growing emphasis on achieving carbon neutrality has led to increasing demand for CO_2 resource utilization technologies. Therefore, CO_2 biomethanation using H_2 produced from surplus electricity has emerged as a promising approach. In the biological route, anaerobic microorganisms convert CO_2 to CH_4 ($CO_2 + 4H_2 \rightarrow CH_4 + 2H_2O$, $\Delta G° = -131$ kJ·mol^{-1}) for energy storage, a process known as "CO_2 biomethanation" (Xirostylidou *et al.* 2024). This process enables the conversion and storage of renewable energy in chemical form, thereby facilitating bidirectional energy exchange between the electricity grid and the natural gas network. The biological route, a key energy storage technology in distributed

multi-energy supply systems, offers significant environmental and economic benefits. However, this technology has not been commercialized due to its low production efficiency and poor system stability for large-scale industrial applications (Santamaría *et al.* 2025).

The low production efficiency of CO_2 biomethanation is mainly attributed to abiotic and biotic limiting factors. Studies have shown that the low gas–liquid mass transfer rate is a key abiotic factor affecting the gas production rate of CO_2 biomethanation (Gonçalves *et al.* 2025). Several studies have focused on reactor design, gas supply methods, and process optimization to enhance gas–liquid mass transfer efficiency (Ghofrani-Isfahani *et al.* 2021; Kalbermatten *et al.* 2025; Ye *et al.* 2026). However, the improvement in gas production efficiency has been limited. In addition to abiotic factors, biotic rate-limiting factors must be taken into consideration. The biotic factors, including microbial community structure, interspecies syntropy, methanogenic pathways, key enzyme activities, and competition among multiple pathways within the microbial consortium, influence methanogenic efficiency. Current strategies for enhancing biotic activity mainly include electrical stimulation and the addition of promoting substances, such as biochar and trace elements (Dong *et al.* 2022; Cristiani *et al.* 2023; Li and Kobayashi 2025).

In anaerobic fermentation, the addition of biochar enhances methanogenesis through multiple synergistic mechanisms (Li *et al.* 2026). Because of its alkali metal content, biochar introduces inherent alkalinity into the liquid phase, thereby shifting the CO_2–carbonate equilibrium toward bicarbonate and carbonate. Additionally, its diverse surface functional groups reversibly bind and release protons. This dual action strengthens the acid–base buffering capacity of the system, stabilizes pH, and accelerates fermentation intermediate conversion. The well-developed porous structure and high specific surface area of biochar enable it to effectively adsorb and precipitate inhibitors, such as H_2S, thus mitigating their detrimental effects on the microbial community. The pore structure of biochar also serves as protective microhabitats for microbial colonization, and the gradual release of carbon, nitrogen, and trace elements from the biochar matrix supplies essential nutrients that enrich and activate the anaerobic consortium. Moreover, during CO_2 biomethanation, a high hydrogen partial pressure can thermodynamically restrict the oxidation of key intermediates and interspecies electron transfer (Wu *et al.* 2025). Biochar, an excellent exogenous conductive material, enables direct interspecies electron transfer (DIET), thereby bypassing the thermodynamic constraint and promoting more efficient methanogenesis (Wang *et al.* 2025).

In the methanogenic stage, anaerobic microbial anabolism depends on macronutrients, including carbon, hydrogen, oxygen, nitrogen, phosphorus, and sulfur, and a suite of essential trace metal elements. These trace elements are incorporated into the cellular component of anaerobic microorganisms and serve as indispensable cofactors in methanogenic biochemistry by participating in the synthesis and activation of key enzymes (Bardi *et al.* 2023). Numerous laboratory studies and operational data from full-scale biogas plants worldwide consistently reveal that a deficiency of the trace elements leads to partial degradation of organic matter, excessive accumulation of VFAs, disruption of acid–base equilibrium, and instability of the process (Shin 2025; Liang *et al.* 2026). In CO_2 biomethanation systems, trace elements are routinely supplemented in the form of nutrient solutions. The result by Moestedt *et al.* showed that appropriately adjusting the mixing ratio of trace-element-rich substrates effectively improved system stability (Moestedt *et al.* 2016). Burkhardt *et al.* supplied essential nutrients, including Co and Ni, to the reactor, achieving a CH_4 concentration of 98% and a maximum volumetric methane production rate (VMP) of 1.49 $L \cdot L_{reactor}^{-1} \cdot d^{-1}$ (Burkhardt *et al.* 2015). Rachbauer *et al.* circulated a

mineral medium containing $NiCl_2$ and other substances, resulting in a CH_4 concentration of 96% and a VMP of 2.52 $L \cdot L_{reactor}^{-1} \cdot d^{-1}$ (Rachbauer *et al.* 2016).

However, the coupled effect of biochar and trace elements is in CO_2 biomethanation—a hydrogenotrophic methanation process with distinct thermodynamic constraints and trace element requirements—remains underexplored. In this study, the effects of biochar and three trace elements (Fe, Co, and Ni) individually on the CO_2 biomethanation process are investigated, and the dosages are optimized using response surface methodology. On this basis, modified biochar was prepared, and its bioenhancement effect and underlying mechanism on CO_2 biomethanation were explored through long-term continuous experiments. Investigating the coupling effect of biochar and trace elements on CO_2 biomethanation provides a theoretical and experimental basis for breaking through the biotic limiting factors of efficient bio-nature gas production.

EXPERIMENTAL

Materials and Methods

Raw materials characterization and biochar preparation

The cattle manure (CM) for fermentation and biochar preparation was collected from a dairy farm in Beijing. The properties of the corn straw (CS) and cattle manure are shown in Table 1. The CS and CM for biochar preparation were dried in an oven at 105 °C for 24 h to remove excess moisture after washing.

Table 1. Raw Material Characteristics

Parameter	Unit	Cattle Manure	Corn Straw	Inoculum
TS	$g \cdot L^{-1}$	203.1 ± 3.7	938.2 ± 4.1	41.9 ± 1.1
VS	$g \cdot L^{-1}$	153.8 ± 3.2	898.3 ± 4.1	30.4 ± 0.9
C	% (DM)	33.96	38.26	/
H	% (DM)	4.23	4.78	/
O	% (DM)	31.78	37.24	/
N	% (DM)	1.74	0.97	/
C/N	/	19.52	39.44	/

Biochar was derived from CS and CM *via* slow pyrolysis in a tubular furnace under an oxygen-limited atmosphere, maintained by a constant N_2 flow of 0.2 $L \cdot min^{-1}$. The pyrolysis process employed final temperatures of 400, 500, and 600 °C, with a heating rate of 10 °C·min^{-1} and a 1 h holding time at each target temperature. The resulting biochars were labeled as CS400, CS500, CS600 (from CS at 400, 500, and 600 °C, respectively) and similarly CM400, CM500, CM600 (from cattle manure at the same temperatures). After pyrolysis, the biochars were cooled to below 100 °C inside the reactor, then transferred to desiccators. The sieved particles were dried at 105 °C for 48 h and stored in airtight plastic bags for subsequent experiments.

The modified biochar

Based on the optimal addition concentrations of various metal elements and the optimal biochar type determined, a mass of 10 g of cattle manure was soaked with 100 mL mixed solution containing $FeCl_2 \cdot 4H_2O$ (15.1 mg $Fe \cdot L^{-1}$), $CoCl_2 \cdot H_2O$ (1.5 mg $Co \cdot L^{-1}$), $NiCl_2 \cdot 6H_2O$ (0.6 mg $Ni \cdot L^{-1}$) for 24 h at room temperature after vibrating for 1 h. Then, it

was filtered and dried for 24 h. The soaking cattle manure underwent pyrolysis at 400 °C in a tubular furnace for 1 h.

Bioaugmentation Experimental Design

Batch experiment

After measuring the Total Solid (TS) and Volatile Solid (VS) content, the cattle manure was diluted with deionized water to a TS content of approximately 60 $g \cdot L^{-1}$, homogenized using a high-speed blender, and stored at -4 °C for later use as the organic feedstock. Batch experiments of the CO_2 biomethanation system were conducted using 120-mL serum bottles. The inoculum was obtained from a stably operated CO_2 biomethanation system in the laboratory. After being filtered through a sieve to remove impurities, it was placed in a 37 °C water bath for later use. A total of 60 mL of inoculum and 10 mL of CM fermentation substrate were added into each 120-mL serum bottle. According to the experimental design, corresponding amounts of trace metal elements and biochar were added to the bottles. The bottles were then purged with nitrogen for 1 min to ensure anaerobic conditions, followed by sealing with butyl rubber and aluminum foil. Using a gas-tight syringe, 40 mL of H_2 and 10 mL of CO_2 mixed gas were injected into the serum bottles of the experimental group, while 50 mL of N_2 was injected into the blank group. All serum bottles were placed in a constant-temperature water bath at 37 °C. The gas production volume and gas composition were measured using a gas-tight syringe.

Biochar obtained from different feedstocks and under different pyrolysis conditions was added at 5% of the total solid content.

In the initial single-element batch experiments, each trace element was added individually to determine its optimal concentration. The concentrations tested were: $FeCl_2 \cdot 4H_2O$ (1, 5, 10, 15, and 20 mg $Fe \cdot L^{-1}$), $CoCl_2 \cdot H_2O$ (0.1, 0.5, 1.0, 1.5, and 2.0 mg $Co \cdot L^{-1}$), and $NiCl_2 \cdot 6H_2O$ (0.1, 0.5, 1.0, 1.5, and 2.0 mg $Ni \cdot L^{-1}$).

Based on these single-element results, the individually optimized concentrations were identified as 15 mg $Fe \cdot L^{-1}$, 1.5 mg $Co \cdot L^{-1}$, and 0.5 mg $Ni \cdot L^{-1}$. Subsequently, mixed-element experiments were conducted using response surface methodology (Box-Behnken design), in which all three trace elements were added together according to the experimental design (Table S1). The concentration ranges for the mixed-element experiments were: Fe (10, 15, 20 $mg \cdot L^{-1}$), Co (1.0, 1.5, 2.0 $mg \cdot L^{-1}$), and Ni (0.1, 0.5, 1.0 $mg \cdot L^{-1}$).

The biochar and trace element batch experiments were conducted independently using different batches of inoculum and cattle manure, which were collected from the same sources but at different time points. The endpoint of each batch experiment was defined as the day when daily methane production fell below 1% of the cumulative production for three consecutive days. After the experiment, the cumulative methane production of each group was calculated and analyzed, and response surface analysis was performed based on the methane production. The Design Expert software (Stat-Ease, Inc., Version 13, Minneapolis, MN, USA) was further used to design experiments with mixed elements. For all batch experiments, three independent biological replicates (n = 3) were performed for each treatment condition with a blank group.

Semi-continuous experiment

The semi-continuous CO_2 biomethanation experiment was conducted in a 5-L continuous stirred-tank reactor (CSTR) with a hydraulic retention time (HRT) of 35 days. The working volume of the reactors was 3.5 L. The ratio of substrate to inoculum was 1:2. In the semi-

continuous anaerobic fermentation, the total solids (TS) concentration of the feed was approximately 15%, while the final TS concentration in the reactor was approximately 6%. The organic load rate (OLR) of was 1.5 g TS $\cdot$ $L^{-1} \cdot d^{-1}$ and the temperature was maintained at 37 ± 1 °C using a water bath. Throughout the experiment, the reactor was fed once daily with dairy manure and gas. The reactor followed the same daily feeding and withdrawal pattern, namely the amount of effluent removed from the reactor was equal to the amount of substrate added to it. A daily feed of 100 mL of cattle manure solution (TS ≈ 15%) was introduced into the reactor. The daily gas loading rates was the volumetric amount of H_2 or CO_2 gas supplied to the reactor per unit reactor working volume per day ($L \cdot Lreactor^{-1} \cdot d^{-1}$). The final amount of H_2 injection was established according to the stoichiometry of hydrogenotrophic methanogenesis reaction: 4 mol of H_2 with 1 mol of CO_2 (from biogas or sum of biogas and additional CO_2). All gas ratios were calculated as normalized volume ratios under standard conditions (0 °C, 101.33 kPa) (Fig. 1).

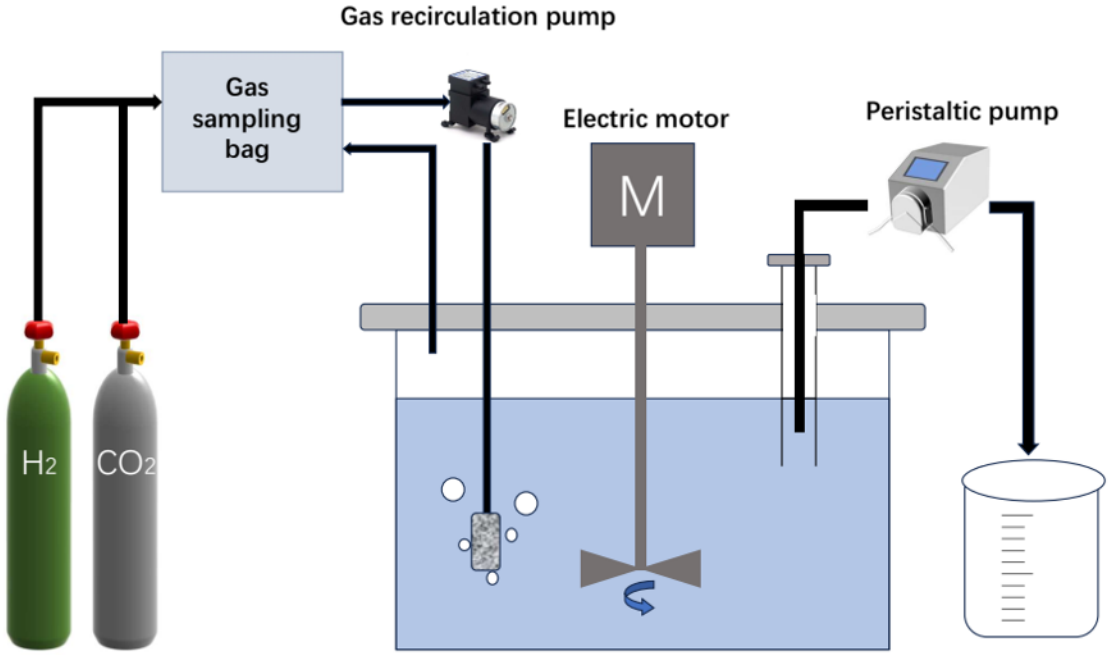

Fig. 1. Diagram of the experimental setup

Agitation speed (0 to 180 rpm) was precisely controlled by a variable-speed motor with a reducer. Feedstock gas was recirculated using a micro gas pump and further dispersed *via* an internal diffuser. Biogas was collected in gas bags. Biogas composition was monitored daily, and biogas yield was recorded using a wet gas meter. The experiment assessed the effect of modified biochar on system performance. Gas composition and yield were measured 24 h after each feeding, while TS, VS, pH, VFAs, and COD were measured every 2 to 3 days.

To further elucidate the influence of the modified biochar on the CO_2 biomethanation system using a before-after control design, a 105-day experiment was conducted comprising a 70-day control phase without biochar addition, followed by a 35-day experimental phase in which the modified biochar was introduced. Throughout both phases, the gas loading rate was dynamically regulated in response to indicators such as methane content and system pH. Through monitoring gas production characteristics,

organic matter degradation, and overall system stability before and after biochar addition, the effect of modified biochar on the CO_2 biomethanation process were systematically assessed.

Analytical Methods

The produced gas yield was measured using a wet gas meter (a positive-displacement drum-type meter sealed with water). Gas composition (CH_4, CO_2, H_2) was analyzed daily by gas chromatography (Shimadzu GC-8A, Japan) equipped with a stainless steel column (10 m × 2 mm i.d.). A 0.5 mL gas sample was collected using a 1-mL syringe and injected into the chromatograph. All gas volumes were corrected to standard conditions (0 °C, 101.33 kPa). The inlet, column, and thermal conductivity detector (TCD) temperatures were 120 °C, 50 °C, and 120 °C, respectively.

The TS and VS were determined following a standard procedure (Greenberg *et al.* 1985). Effluent samples were collected every 2 to 3 days to measure pH, total COD (TCOD), soluble COD (SCOD), and volatile fatty acids (VFAs). The pH was measured using a pH meter (Mettler-Toledo, USA). For SCOD analysis, feedstock and effluent samples were centrifuged at 8000 rpm for 20 min using a high-speed refrigerated centrifuge (TGL-16 M, China). The supernatant was then filtered through a 0.45-μm membrane. Both TCOD and SCOD were measured using Lianhua LH-DE500 reagent *via* the fast digestion-spectrophotometric method (Chinese standard GB/T 32208-2015) at 610 nm.

The VFAs were analyzed using a gas chromatograph (Shimadzu GC-2010 Plus, Japan). The soluble fraction of the samples was filtered through a 0.45-μm microfiber filter, and the filtrate was injected (1.0 μL) into a DB-wax capillary column (30 m × 530 mm × 1.0 μm) with a flame ionization detector. The injector and detector temperatures were 200 and 250 °C, respectively. Nitrogen was used as the carrier gas at a flow rate of 10 $mL \cdot min^{-1}$. All analytical measurements were performed in triplicate, and data are reported as means ± SD where applicable.

The samples for microbial analysis were collected during stable periods of different reaction stages: on days 24 and 51 of the control phase, and on days 79 and 102 after the addition of modified biochar. These samples were designated D24, D51, D79, and D102, respectively. Each sample was sealed in a 50-mL centrifuge tube and stored at −80 °C.

The microbial community analysis was conducted by Shanghai Majorbio Bio-pharm Technology Co., Ltd. Operational taxonomic units (OTUs) and their relative abundances were derived from 16S rRNA sequencing data to ensure accurate taxonomic classification and quantification. The methods for bacterial and archaeal analysis followed our previous study (Ye *et al.* 2026), and data were analyzed using the Majorbio Cloud Platform (www.majorbio.com).

Statistical Analysis of Data

Data were collated, analyzed, and plotted and the correlation analysis plots were generated using Origin Pro 2021. For the batch experiments, one-way analysis of variance (ANOVA) was performed using IBM SPSS Statistics 27, followed by Dunnett's t-test (two-tailed) for post-hoc multiple comparisons between each treatment group and the control group. A significance threshold of $\alpha = 0.05$ was applied. For the response surface methodology, Design-Expert 13 was used to perform ANOVA on the quadratic regression model, and the model-predicted optimum was validated against experimental results using a two-tailed paired t-test.

RESULTS AND DISCUSSION

Effects of Biochars on CO_2 Biomethanation Systems

Gas production performance

The effects of different biochars derived from two distinct feedstocks under various pyrolysis temperatures on CO_2 biomethanation systems were investigated (Fig. 2 Biochar).

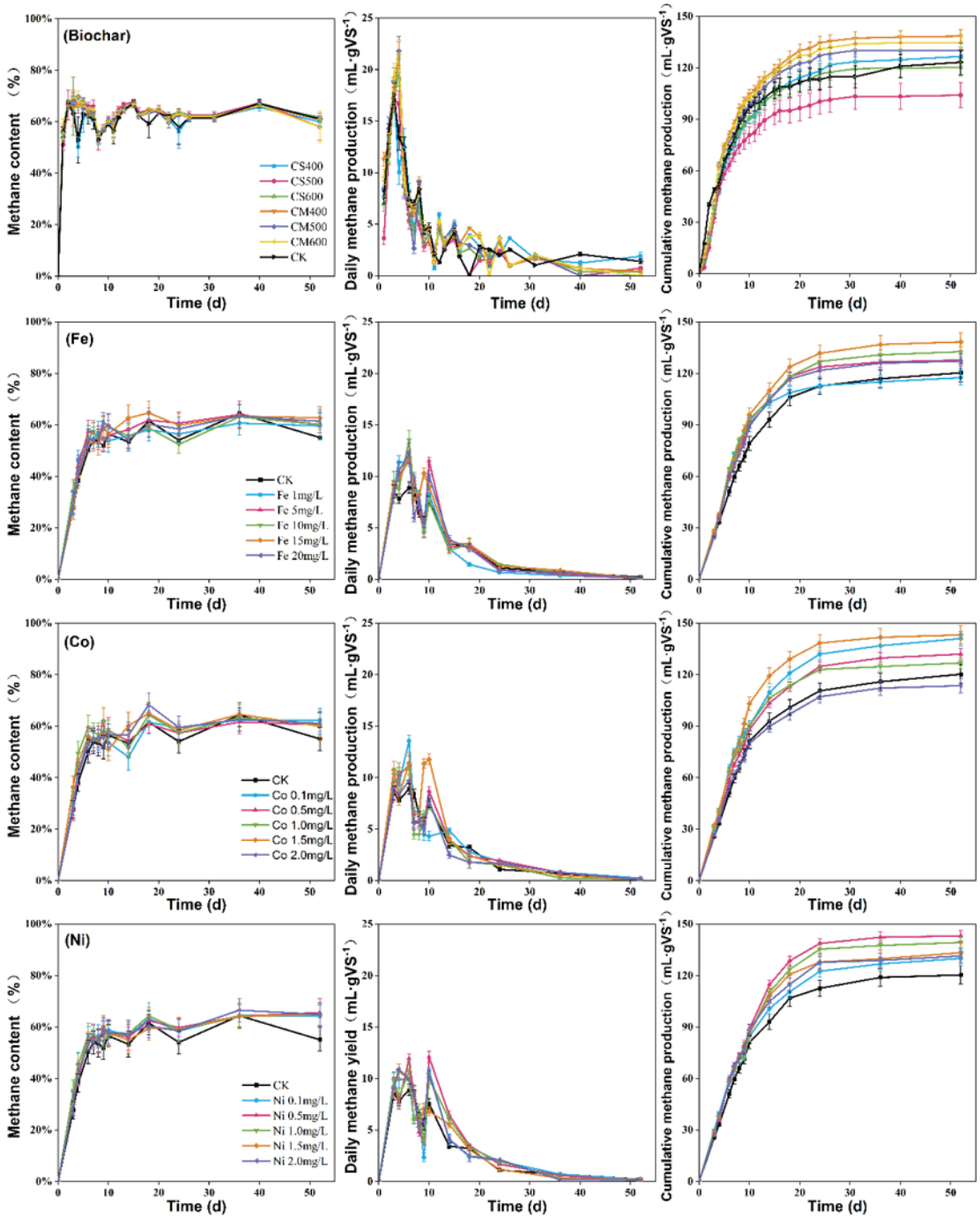

Fig. 2. Methane production performance of the system after biochar or trace elements addition in batch experiment

All groups exhibited a distinct peak in gas production during the early stage of the batch experiment, and the cumulative methane yield linearly increased. On day 3, the daily methane yield of the control group peaked at 17.6 mL·gVS^{-1}. The daily methane yields of three CS biochar groups peaked on days 3, 3, and 4, resulting in 17.8, 17.2, and 19.8 mL·gVS^{-1}, respectively. The daily methane yields of CM biochar groups on day 4 peaked at 21.4, 21.8, and 21.4 mL·gVS^{-1}, which were 21.8%, 24%, and 21.7% higher than that of the control, respectively. After day 18, the methanogenesis rate slowed considerably across all groups, and the rate of increase in cumulative methane yield decreased, with the reaction terminating on day 50. The final cumulative methane yield of the control group was approximately 123 mL·gVS^{-1}. The addition of CM biochars modestly enhanced cumulative methane production. This enhancement was more pronounced in the CM400 group, which achieved a final cumulative methane yield of 138 mL·gVS^{-1}. Compared with the control, cumulative methane yields increased 12.1%, 8.1%, and 9.8% in the CM400, CM500, and CM600 groups, respectively. This enhancement might be attributed to the abundance of redox-active functional groups in CM biochar produced under low-temperature pyrolysis. The functional group facilitated electron transfer through redox reactions and interspecies electron transfer among microorganisms, thereby enhancing methanogenesis (Bu *et al.* 2022). The CS biochar groups yielded low gas, consistent with the finding of Pan *et al.*, who reported that biochars derived from chicken manure and fruitwood achieved higher methane yield improvements than CS biochar (Pan *et al.* 2019). Biochar slightly increased the methane content in the reactors relative to the control, and the methane content in the CM600 group peaked at 71.9% on day 3, representing an increase of 7.2% over the control.

Metabolic performance

Figure 3 (a) shows the effects of different CS biochars on the removal efficiencies of TS, VS, and TCOD in the CO_2 biomethanation system. No significant differences ($p > 0.05$) in the removal efficiencies of TS, VS, and TCOD were observed between the CS400, CS500, and the control groups. This slight difference may be attributed to the relatively low pyrolysis temperature used for the straw-based feedstock. This low pyrolysis temperature may result in incomplete carbonization, underdeveloped pore structures, and unstable physicochemical properties, thereby limiting the ability to effectively promote organic matter degradation. In contrast, the CS600 group exhibited higher removal efficiencies of TS, VS, and TCOD than the control, reaching 35.7, 38.7, and 41.3%, respectively, increasing 9.8, 12.5, and 7.0% relative to the control.

Figure 3 (b) illustrates the organic matter removal efficiencies in the groups supplemented with different CM biochars. Compared with the control group, the TS, VS, and TCOD removal efficiencies of all CM biochar groups significantly increased ($p < 0.05$). Among the groups, the CM400 group achieved the highest organic matter removal efficiencies, with TS, VS, and TCOD removal rates of 41.0, 46.3, and 49.0%, respectively, which were 26.2, 34.6, and 26.9% higher than those of the control. In the CM500 and CM600 groups, the TCOD removal efficiencies were 48.2% and 45.6%, respectively, corresponding to increases of 24.4% and 18.1%.

The addition of biochar led to varying degrees of improvement in H_2 consumption rate, cumulative methane yield, and organic matter removal efficiency compared with the control group. These results showed that the favorable physicochemical properties of biochar effectively stimulated microbial enrichment and activity, thereby enhancing digestion performance and the metabolic activity of methanogenic archaea (Yuan *et al.*

2018). Furthermore, the electrical conductivity of biochar may also play a role in facilitating interspecies electron transfer among microorganisms.

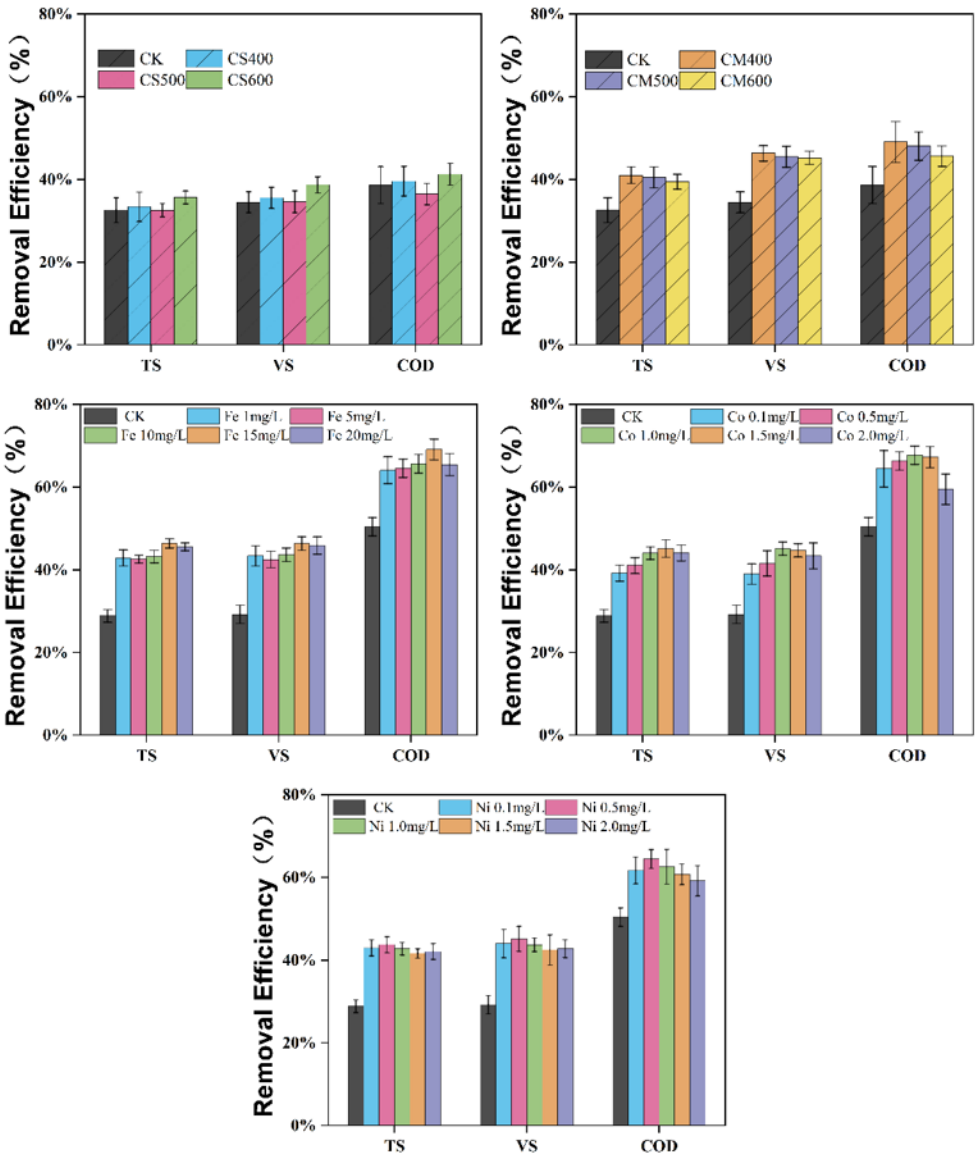

Fig. 3. Removal efficiencies (%) of organic matter after biochar or trace elements addition in batch experiment: (a) CS biochar addition individual; (b) CM biochar addition individual; (c) Fe addition individual; (d) Co addition individual; (e) Ni addition individual

Effects of Trace Elements on the CO_2 Biomethanation System

Gas production performance

Fe is the most abundant metal element in methanogenic cells and plays essential roles in the synthesis of various enzymes during methanogenesis (Gong *et al.* 2026). The effects of different concentrations of Fe on the gas production of the CO_2 biomethanation system are shown in Fig. 2 (Fe). On day 6, the daily methane yield of the control group peaked at 8.91 mL·gVS^{-1}. The cumulative methane yield of the control group was 120 mL·gVS^{-1} after 52 days. In the Fe-supplemented groups, the highest cumulative methane

yields were 138.4 mL·gVS^{-1}, which was 15.3% higher than those of the control group at 15 mg·L^{-1}. The observed increases in methane content and cumulative methane yield may be attributed to the positive effects of Fe on various bacteria and enzymes involved in the CO_2 biomethanation process. The average methane contents in the control group and Fe-supplemented groups were 51.7% and 53.5 to 55.2%, respectively. This represented a slight increase compared with that in the control group.

As an essential component of acetogenic and methanogenic microorganisms, Co addition significantly enhanced gas production (Méndez-Contreras *et al.* 2024). Figure 2 (Co) shows the effects of different concentrations of Co on the gas production performance. Compared with the control, Co addition also increased both daily methane yield and cumulative methane yield. The enhancements were more pronounced at Co concentrations of 0.1 mg·L^{-1} and 1.5 mg·L^{-1}. The highest daily methane yield of 13.6 mL·gVS^{-1} was observed at a Co concentration of 0.1 mg·L^{-1}, representing a 52.4% increase over the control. The peak cumulative methane yield of 143.3 mL·gVS^{-1} was achieved at a Co concentration of 1.5 mg·L^{-1}, corresponding to a 19.38% increase over the control. However, at a Co concentration of 2.0 mg·L^{-1}, the cumulative methane yield was lower than that of the control, possibly due to the toxic effects of excessive Co on methanogenic microorganisms, which consequently reduced methane production (Šafarič *et al.* 2020).

Ni serves as an essential cofactor for key methanogenic enzymes, including hydrogenases and carbon monoxide dehydrogenase/acetyl-CoA synthase, thereby promoting the CO_2 biomethanation process (Ramírez-Amador *et al.* 2025). Figure 2 (Ni) shows the effects of different concentrations of Ni on the gas production performance. Similar to the effects observed with Fe and Co, the presence of Ni significantly enhanced methanogenic performance. Ni also improved both daily methane yield and cumulative methane yield. The optimal daily methane yield of 12.1 mL·gVS^{-1} was observed at a Ni concentration of 0.5 mg·L^{-1}, and the cumulative methane yield peaked at 143.1 mL·gVS^{-1} at the same concentration, which was 19.2% higher than that of the control.

Metabolic performance

The effects of Fe, Co, and Ni on the organic matter removal efficiency are shown in Fig. 3 (c, d, and e). Compared with the control group, all supplemented groups exhibited significant differences in removal efficiencies ($p < 0.05$). The TCOD removal efficiency in the control group was 50.4%. The Fe-supplemented group exhibited optimal TCOD removal efficiency of 69.1% at a Fe concentration of 15 mg·L^{-1}, which was 37.1% higher than that of the control. Co significantly enhanced organic matter removal efficiency. The maximum TCOD removal efficiencies of 67.7% and 64.5% were achieved at Co and Ni concentrations of 1.0 mg·L^{-1} and 0.5 mg·L^{-1}, respectively, which were 34.3% higher than those in the control group. The COD removal efficiencies obtained in the three trace element experiments were higher than those of the control group in the CO_2 biomethanation experiment. This disparity indicates that trace elements can alleviate the inhibition of organic matter degradation during CO_2 biomethanation.

The batch experiments on CO_2 biomethanation revealed that the addition of individual trace elements indeed facilitated the methanogenesis process to a certain extent. Among the trace elements, Fe, as one of the most critical elements in the synthesis and physiological metabolism of methanogenic cells, facilitated the production of VFAs and enhanced the utilization efficiency of methanogens for intermediates such as acetate (Suanon *et al.* 2016). Co, as an essential component of methyltransferases and carbon monoxide dehydrogenases, effectively increased the biological activity of methanogens

and microorganisms such as *Methanosarcina barkeri*. Ni played an important role in the process of H_2 reduction of CO_2 to CH_4. Recent research has demonstrated that co-supplementation of multiple trace elements is more effective than mono-supplementation. a study using response surface methodology found that co-supplemented Fe, Co, and Ni achieved a 27.4% increase in methane yield under optimal conditions (Fe: 113.1, Co: 0.51, Ni: 2.44 mg/L) (Zhu *et al.* 2024). Another study reported that Ni^{2+} (1 mg/L) + Co^{2+} supplementation increased methane yield by 14% and 12%, respectively (Salazar-Batres and Moreno-Andrade 2025). However, during CO_2 biomethanation, trace elements did not act independently in physiological metabolism, but multiple trace elements synergistically interacted and collectively functioned to ensure the smooth progression of the overall methanogenesis process.

Effects of mixed trace elements on biomethanation systems

The single-factor experimental results of the effect of individual addition of trace elements described in the previous section revealed that the highest cumulative methane yields were achieved at concentrations of 15 mg·L^{-1} for Fe, 1.5 mg·L^{-1} for Co, and 0.5 mg·L^{-1} for Ni. As a result, Fe, Co, and Ni were selected as independent variables, and cumulative methane yield was selected as the response variable. Concentration gradients were set as follows: Fe (10, 15, and 20 mg·L^{-1}), Co (1.0, 1.5, and 2.0 mg·L^{-1}), and Ni (0.1, 0.5, and 1.0 mg·L^{-1}). A three-factor, three-level response surface methodology was designed using Design Expert software, comprising a total of 17 experimental points. The experimental factor levels and coding are shown in Table S1.

The specific experimental procedures for the mixed-element experiments were the same as those for the single-element experiments. The experimental results are presented in Table S2. Using Design Expert software, a quadratic polynomial regression equation was developed based on the aforementioned experimental levels and independent variables, with the cumulative methane yield Y as the response variable and concentration of Fe, Co, and Ni as the independent variables.

$$Y = 132.61 + 0.4030 \times A + 0.8688 \times B + 0.8315 \times C + 0.0175 \times AB$$
$$-0.3000 \times AC + 0.0420 \times BC - 7.33 \times A^2 - 10.74 \times B^2 - 4.58 \times C^2 \quad (1)$$

In Eq. 1, Y is the cumulative methane yield (mL·gVS^{-1}), A means Fe concentration (mg·L^{-1}), B means Co concentration (mg·L^{-1}), C means Ni concentration (mg·L^{-1}), A^2, B^2, and C^2 mean quadratic terms representing the curvature (non-linear effects) of each trace element, and AB, AC, and BC mean interaction terms representing the synergistic or antagonistic effects between pairs of trace elements.

The RSM regression model was statistically significant ($p < 0.0001$, $R^2 = 0.9761$), indicating that the model adequately described the response data. However, ANOVA of the individual model terms (Table S3) revealed that only the quadratic terms (A^2, B^2, C^2) were statistically significant ($p < 0.01$), while all linear terms (A, B, C) and interaction terms (AB, AC, BC) were not significant ($p > 0.05$). This indicates that the influence of Fe, Co, and Ni on cumulative methane yield was predominantly curvilinear—*i.e.*, each element exhibited an optimal concentration range—rather than simply linear or interactive. The model predicted an optimal trace element combination (Fe: 15.1 mg·L^{-1}, Co: 1.5 mg·L^{-1}, Ni: 0.6 mg·L^{-1}) that was experimentally validated, confirming that the quadratic model provides a useful predictive framework despite the non-significant linear and interaction terms.

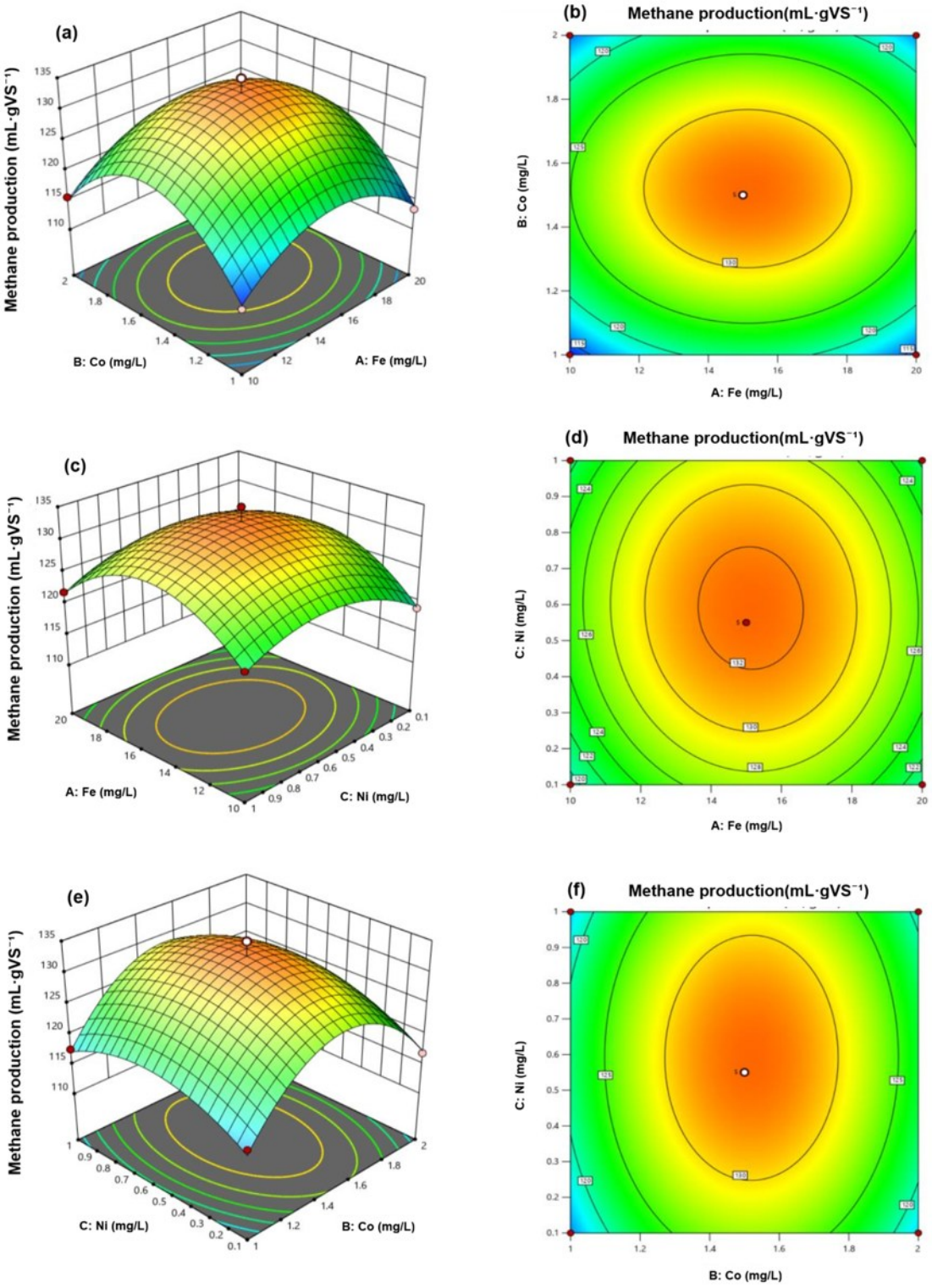

Fig. 4. Effect of different trace element interactions on cumulative methane production
Note: (a, c, e) are the 3D response surface analyses, and (b, d, f) are the top views

The steepness of the response surface curves visually reflected the magnitude of factor interactions, exhibiting a positive correlation. Notably, a steeper surface slope reflects in a stronger corresponding interaction effect; conversely, a flatter surface indicates a weaker interaction. Figure 4 shows the effects of each factor and their interactions on cumulative methane yield. The response surface curve for the interaction between B and C was the steepest, indicating that Co and Ni had the most significant influence on cumulative methane yield. The interaction between A and C was moderately strong, while the interaction between A and B was relatively weak. This trend was confirmed by the contour plots: the B–C contour exhibited a distinct elliptical shape, indicating a strong interaction. In contrast, the A–B contour was almost circular, reflecting a weaker interaction. Based on the experimental data and graphical analysis, the order of interaction strength was BC > AC > AB.

In summary, the response surface analysis identified a combination of trace elements that maximized cumulative methane yield. Using Design Expert software and considering practical conditions, the optimal fermentation conditions were identified as Fe at 15.1 $mg \cdot L^{-1}$, Co at 1.5 $mg \cdot L^{-1}$, and Ni at 0.6 $mg \cdot L^{-1}$. Under these conditions, the predicted cumulative methane yield was predicted to be 132.7 $mL \cdot gVS^{-1}$. Based on the response surface analysis results and optimized concentrations identified in the single-factor experiments, validation experiments were conducted using Fe at 15.1 $mg \cdot L^{-1}$, Co at 1.5 $mg \cdot L^{-1}$, and Ni at 0.6 $mg \cdot L^{-1}$. The cumulative methane yield achieved in the validation experiments was 135.5 $mL \cdot gVS^{-1}$. No significant difference was observed between the validation experiments and the predicted value, confirming the reliability of the experimental results.

Effects of Trace Element-loaded Biochar on the CO_2 Biomethanation

Gas production performance

The gas production performance of the system before and after the addition of modified biochar is shown in Fig. 5. Throughout the experiment, the feed concentration was maintained at a TS of 6%. During days 0 to 70 (corresponding to the control phase, without modified biochar), the initial H_2 and CO_2 loading rates were 1.71 $L_{H2} \cdot L_{reactor}^{-1} \cdot d^{-1}$ and 0.19 $L_{CO2} \cdot L_{reactor}^{-1} \cdot d^{-1}$, respectively. The CH_4 content in the reactor was approximately 86%, and the VMP was 0.71 $L_{CH_4} \cdot L_{reactor}^{-1} \cdot d^{-1}$. Subsequently, the CH_4 content fluctuated between 73 % and 91 % during the control phase (days 0 to 70), depending on the gas loading rate and operational disturbances, with the peak value of 91 % recorded on day 51 before H_2 accumulation occurred. During operation, the H_2 and CO_2 loading rates were adjusted according to daily gas consumption. On day 25, the CH_4 content in the reactor decreased to 73% due to a malfunction in the gas circulation device. As a result, the H_2 and CO_2 loading rates were reduced, and the system returned to normal after 5 days. On day 51, the H_2 loading rate of the reactor increased to 2 $L_{H2} \cdot L_{reactor}^{-1} \cdot d^{-1}$, thus decreasing the CH_4 content from 91% to 62%, with the proportion of unconsumed H_2 reaching 23%. This phenomenon indicated that the reactor had reached its H_2 consumption limit, and the VMP was 0.69 $L_{CH_4} \cdot L_{reactor}^{-1} \cdot d^{-1}$. After H_2 accumulation, the daily gas loading rates were reduced, and the CH_4 content gradually recovered to approximately 80%, with the VMP maintained at approximately 0.73 $L_{CH_4} \cdot L_{reactor}^{-1} \cdot d^{-1}$. During the control phase (days 0 to 70), the highest H_2 and CO_2 loading rates were 2 $L_{H2} \cdot L_{reactor}^{-1} \cdot d^{-1}$ and 0.29 $L_{CO2} \cdot L_{reactor}^{-1} \cdot d^{-1}$, respectively, and the maximum VMP was 0.81 $L_{CH_4} \cdot L_{reactor}^{-1} \cdot d^{-1}$.

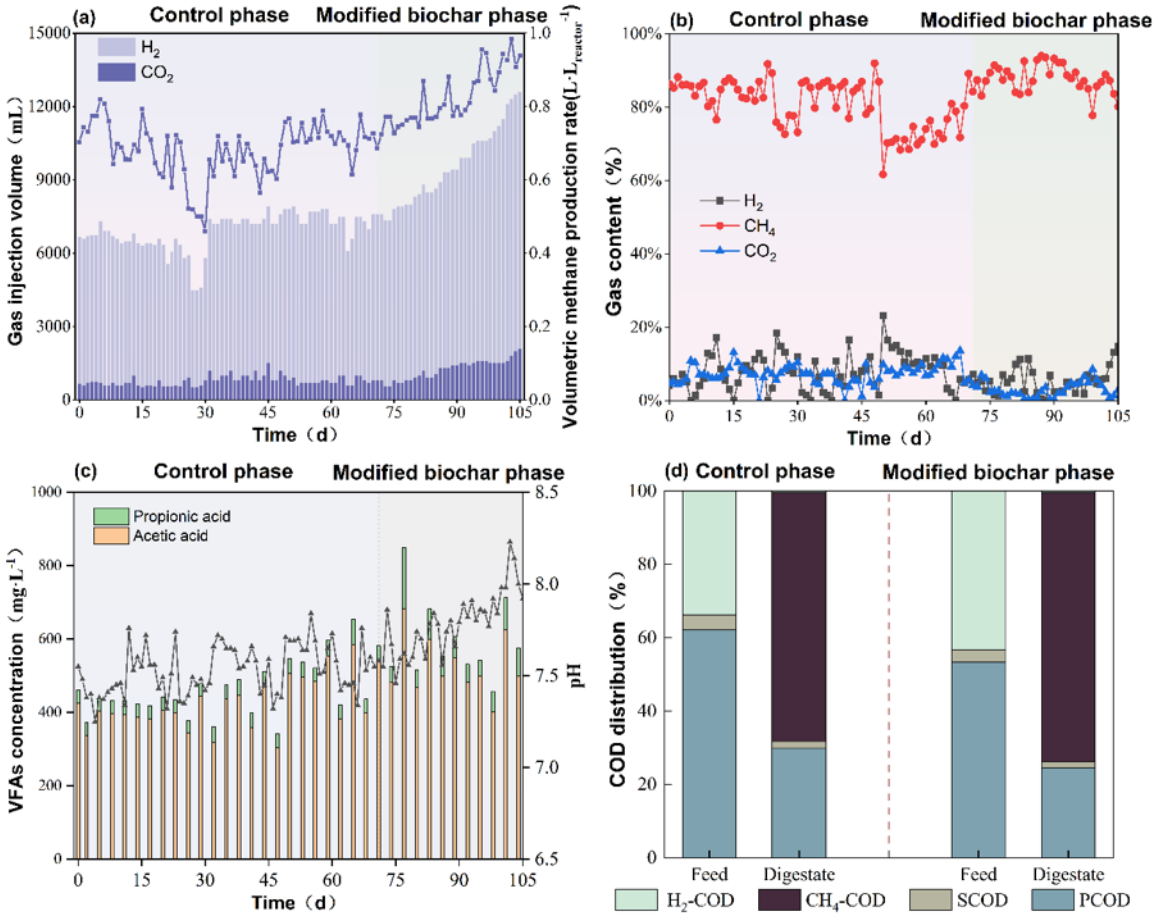

Fig. 5. The gas production performance of Semi-continuous experiment: (a) VMP; (b) gas content; (c) VFA concentration; (d) COD distribution

On day 71, modified biochar was introduced to the reactor at an amount equivalent to 5% of the TS content in the reactor and was subsequently replenished every 3 to 5 days to maintain a stable effective concentration of the modified biochar in the reactor. The gas loading rates were gradually increased while maintaining complete daily consumption of H_2 and CO_2, and stable VFA concentrations and pH. During this phase, both the CH_4 content and the VMP significantly increased. This improvement may be attributed to the excellent electrical conductivity of biochar, which can facilitate electron transfer during the reaction and accelerate the reaction rate. Additionally, trace elements, such as Fe, Co, and Ni, enhanced the activity of anaerobic microorganisms, further accelerating the methanogenesis rate. On day 103, the CH_4 content was 86%, and the VMP peaked at approximately 0.97 $L_{CH_4} \cdot L_{reactor}^{-1} \cdot d^{-1}$, which was 19.8% higher than the phase without modified biochar. Meanwhile, the H_2 and CO_2 loading rates in the reactor were 3 $L_{H2} \cdot L_{reactor}^{-1} \cdot d^{-1}$ and 0.51 $L_{CO2} \cdot L_{reactor}^{-1} \cdot d^{-1}$, respectively, which were 50% and 75.9% higher than those in the control phase without modified biochar.

Metabolic performance

During CO_2 biomethanation, the pH of the system was regulated by buffering components, including CO_2, HCO_3^-, and phosphates. When CO_2 and other compounds were consumed, the buffering capacity of the system was affected, thereby influencing the

metabolic activity of the relevant microorganisms. The pH and VFA concentrations in the reactor during the process are shown in Fig. 5 (c).

During the experimental phase with modified biochar, VFA concentration slightly increased to 849 $mg \cdot L^{-1}$ in the initial stage, accompanied by a moderate increase in pH. This phenomenon can be attributed to the accelerated hydrolysis and acidification rates after the addition of modified biochar and the reaction of metal cations, such as Fe, present on the biochar in the digestate, imparting weak alkalinity. After 9 days of continued reaction, a portion of the organic acids was degraded, reducing the VFA concentration in the reactor to 516 $mg \cdot L^{-1}$. A transient increase in VFAs occurred on day 103, coinciding with the increase in H_2 loading rate to 3.0 $L \cdot L^{-1} \cdot d^{-1}$. This observation is mechanistically consistent with the known thermodynamic inhibition of syntrophic VFA oxidation under elevated H_2 partial pressure. However, the increase was modest (849 $mg \cdot L^{-1}$) and was followed by a rapid decline to 516 $mg \cdot L^{-1}$, indicating that the conductive biochar, by facilitating DIET, effectively provided an alternative electron transfer route that circumvented the thermodynamic constraint. Thus, while high H_2 partial pressure transiently perturbed the system, the DIET-enabled syntrophic pathway, together with the chemical buffering capacity of the modified biochar, prevented sustained VFA accumulation and ensured stable methanogenesis (Zhao *et al.* 2025).

Figure 5(d) shows the effect of modified biochar addition on organic matter removal efficiency in the reaction system. During system operation, the feed TS concentration was 6%, and the TCOD was 98.6 $gCOD \cdot L^{-1}$. In the phase without biochar, the removal efficiencies of TS, VS, and TCOD were approximately 37.9, 36.9, and 52.7%, respectively. After the modified biochar was introduced into the system with increasing H_2 and CO_2 loading rates, microbial community analysis revealed enrichment of electroactive bacteria (Synergistota, Chloroflexota, DMER64, Thermovirga) and DIET-capable methanogens (Methanothrix), which is consistent with the hypothesis that the conductive biochar matrix may facilitate interspecies electron transfer among microorganisms (Han *et al.* 2025b). Consequently, organic matter removal efficiencies improved markedly, with TS, VS, and TCOD removal efficiencies reaching 44.7, 44.6, and 54.5%, respectively. Although the organic matter removal efficiency remained lower than that of conventional anaerobic digestion after adding biochar, TS, VS, and TCOD increased 21.1, 20.9, and 3.4%, respectively, compared with the phase without biochar addition. These results show that modified biochar can alleviate the inhibitory effect of H_2 on organic matter metabolism. In addition, the increased reduction of TS, VS, and COD may result from improved substrate utilization and enhanced anaerobic digestion performance due to the supplementation of essential elements.

Effect of Trace Element-loaded Biochar on Microbial Communities

Alpha diversity analysis of microbial communities

Alpha diversity analysis refers to the quantitative description of microbial diversity within a single sample using a series of indices (such as Ace, Chao, Shannon, Simpson, and Sobs), reflecting the species composition of the community from multiple dimensions, including richness, evenness, and diversity. Table 2 shows the alpha diversity of bacteria at different stages. Coverage represents the library coverage of the experimental samples. All groups exhibited coverage values exceeding 99%, indicating a high probability of sequence detection and that the analytical results adequately reflect the microbial community.

Table 2. Alpha Diversity of Bacterial and Archaeal Communities at Different Stages

		Sample (d)	Ace	Chao	Shannon	Simpson	Coverage	Sobs
Bacterial Vommunities	Control phase	27	800.56	790.68	4.4583	0.0326	0.99747	720
		51	801.29	782.62	4.2693	0.0381	0.9972	702
	Modified biochar addition	79	853.71	831.12	4.4114	0.0333	0.9972	765
		102	843.13	820.34	4.6383	0.0239	0.9979	790
Archaeal Communities	Control phase	27	57.73	57.5	1.3212	0.4874	0.9998	56
		51	48.23	48	1.3198	0.4814	0.9999	48
	Modified biochar addition	79	54.15	53.05	1.3168	0.5100	0.9999	53
		102	57.23	55.11	1.6082	0.3687	0.9998	54

The Ace and Chao indices are indicators of species richness, which reflect the total number or estimated total number of species in a sample without considering species abundance distribution. Shannon and Simpson indices are used to assess microbial community diversity. The alpha diversity analysis results indicate that the addition of modified biochar was associated with increased community evenness and the emergence of new phylotypes. These structural changes are considered functionally favorable in the context of this system because they coincided with—and are mechanistically consistent with—the observed improvements in VMP (+19.8%), H_2 loading capacity (+50%), organic matter removal (TS: +21.1%, VS: +20.9%), and system stability (maintained pH and low VFA concentrations). The Ace and Chao indices slightly increased after the addition of modified biochar, and the Shannon index increased from 4.27 to 4.64 while the Simpson index decreased from 0.038 to 0.024. These changes suggest a shift in community structure toward greater evenness and the emergence of new phylotypes, which is consistent with the selective enrichment of functional guilds under the modified biochar regime.

During the control phase, the Ace and Chao indices of the archaeal community decreased slightly (from 57.73 to 48.23 and from 57.50 to 48.00, respectively), while the Shannon index remained relatively stable. These changes suggest a modest reduction in archaeal species richness over time under continuous H_2/CO_2 feeding conditions, which may reflect the adaptation of the community to the selective pressure of sustained hydrogenotrophic methanogenesis.

Following the addition of modified biochar (days 71–105), the Ace and Chao indices increased to 57.23 and 55.11, respectively, and the Shannon index rose from 1.32 to 1.6, while the Simpson index decreased from 0.48 to 0.37. This pattern—higher Shannon and lower Simpson values—indicates an association between modified biochar addition and increased archaeal community evenness and diversity.

Venn diagrams of the reaction system at different stages are shown in Fig. 6. The Venn diagram analysis revealed 461 OTUs shared between the control phase and the modified biochar addition phase, out of which 135 OTUs were unique to the control phase and 211 OTUs were unique to the modified biochar addition phase. The number of archaeal OTUs was lower than that of bacterial OTUs, with only 43 OTUs shared between the two phases. After the addition of modified biochar, the CO_2 biomethanation system exhibited a greater number of unique OTUs and higher microbial diversity, consistent with the alpha diversity analysis results using various indices.

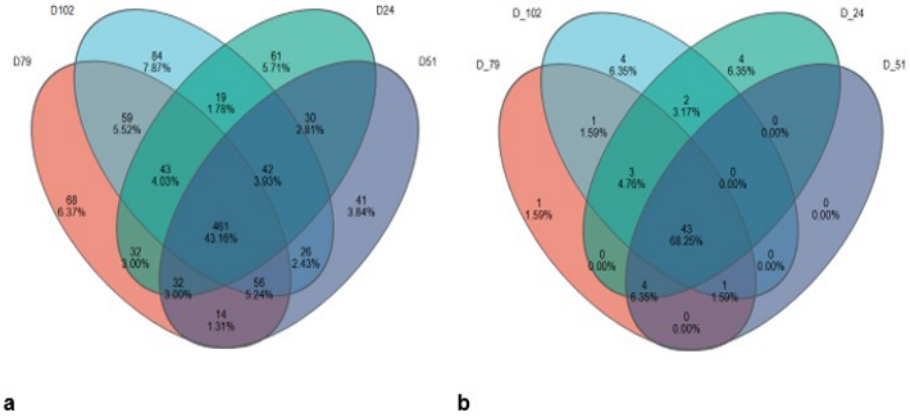

Fig. 6. Venn plot under different reaction stages (bacteria, a; Archaea, b)

Bacterial community analysis

During CO_2 biomethanation, different bacterial communities decomposed organic matter and produced metabolites such as CH_4. The relative abundances of bacterial communities at the phylum level across different stages are shown in Fig. 7 (a). Before and after the addition of modified biochar, abundances of *Bacillota* and *Bacteroidota* remained relatively high. Relevant studies have shown that both phyla influence the hydrolysis and acidification of organic matter (Zhou *et al.* 2024). Notably, *Bacillota* secrete cellulases, hemicellulases, proteases, and other enzymes that degrade macromolecular organic matter into soluble small molecules and subsequently promote the production of VFAs during the acidification stage (Zheng *et al.* 2025). *Bacteroidota* participate in the decomposition of plant-derived polysaccharides (such as cellulose, hemicellulose, and pectin) by secreting large amounts of extracellular enzymes, including cellulases (Wang *et al.* 2026). Some species within the phylum also degrade nitrogen-containing organic compounds. After the addition of modified biochar, the relative abundances of *Bacillota* and *Bacteroidota* slightly decreased from 43.2% and 31.0% to 35.5% and 25.7%, respectively, thereby affecting the hydrolysis of organic matter.

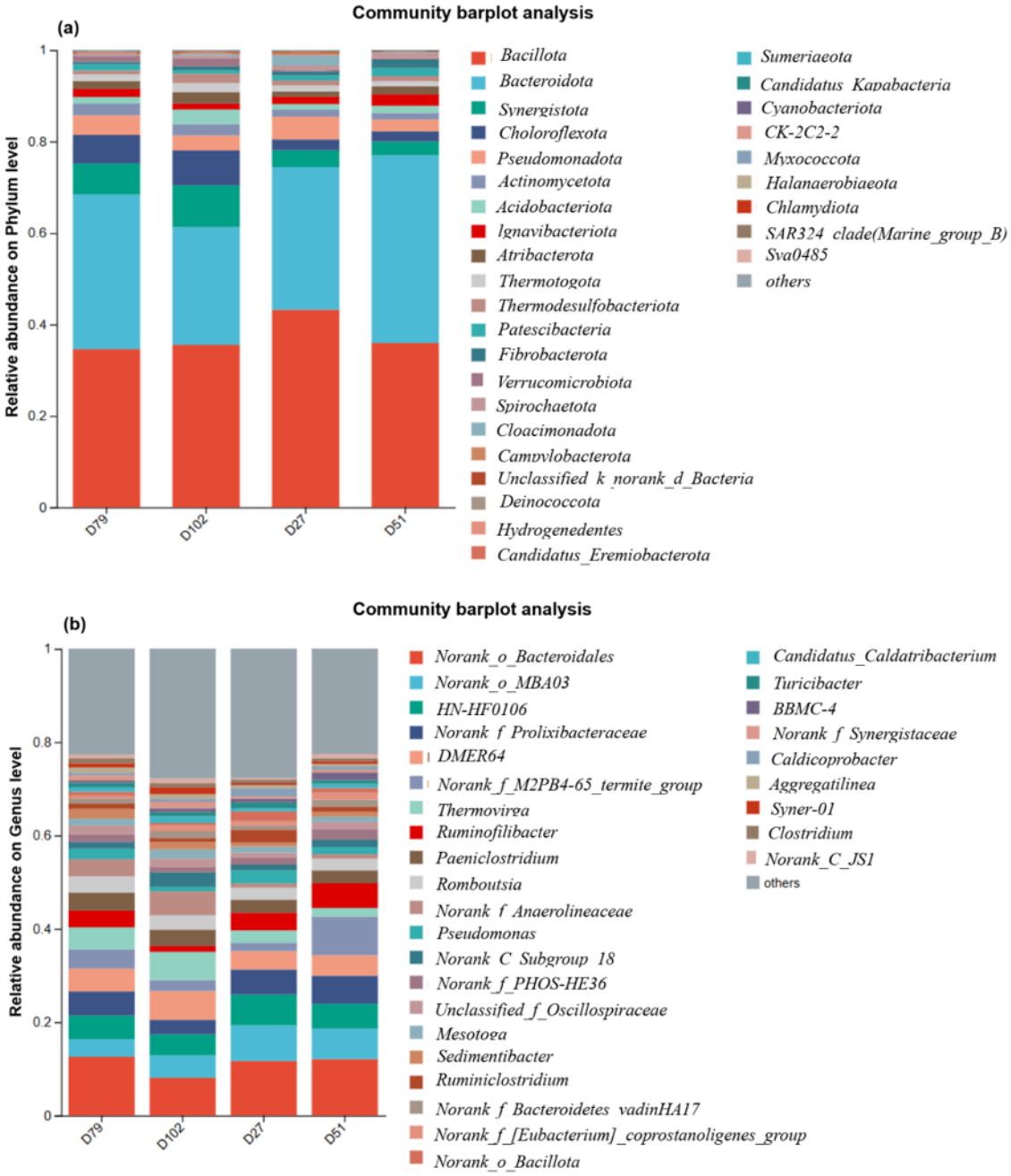
Community barplot analysis
(a)
Relative abundance on Phylum level
1
0.8
0.6
0.4
0.2
0
D79
D102
D27
D51
Bacillota
Bacteroidota
Synergistota
Choloroflexota
Pseudomonadota
Actinomycetota
Acidobacteriota
Ignavibacteriota
Atribacterota
Thermotogota
Thermodesulfobacteriota
Patescibacteria
Fibrobacterota
Verrucomicrobiota
Spirochaetota
Cloacimonadota
Campylobacterota
Unclassified_k_norank_d_Bacteria
Deinococcota
Hydrogenedentes
Candidatus_Eremiobacterota
Sumeriaeota
Candidatus_Kapabacteria
Cyanobacteriota
CK-2C2-2
Myxococcota
Halanaerobiaeota
Chlamydiota
SAR324_clade(Marine_group_B)
Sva0485
others
Community barplot analysis
(b)
Relative abundance on Genus level
1
0.8
0.6
0.4
0.2
0
D79
D102
D27
D51
Norank_o_Bacteroidales
Norank_o_MBA03
HN-HF0106
Norank_f_Prolixibacteraceae
DMER64
Norank_f_M2PB4-65_termite_group
Thermovirga
Ruminofilibacter
Paeniclostridium
Romboutsia
Norank_f_Anaerolineaceae
Pseudomonas
Norank_C_Subgroup_18
Norank_f_PHOS-HE36
Unclassified_f_Oscillospiraceae
Mesotoga
Sedimentibacter
Ruminiclostridium
Norank_f_Bacteroidetes_vadinHA17
Norank_f_[Eubacterium]_coprostanoligenes_group
Norank_o_Bacillota
Candidatus_Caldatribacterium
Turicibacter
BBMC-4
Norank_f_Synergistaceae
Caldicoprobacter
Aggregatilinea
Syner-01
Clostridium
Norank_C_JS1
others

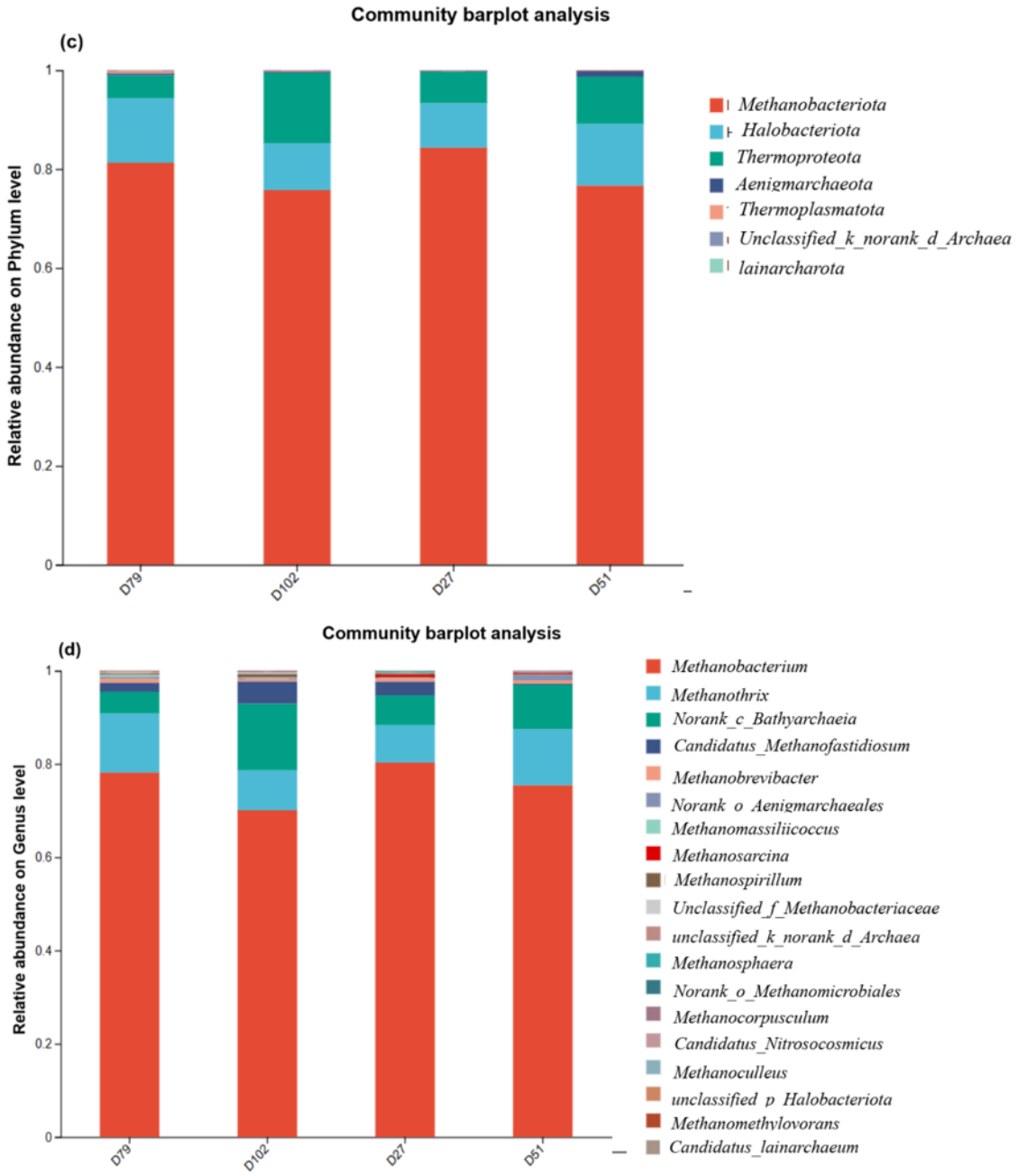

Fig. 7. Relative abundance of Microbial Communities at different stages: (a) Bacterial Communities in phylum level; (b) Bacterial Communities in genus level; (c) Archaea Communities in phylum level; (d) Archaea Communities in genus level

Synergistota are anaerobic bacteria that cooperate with other microorganisms (such as methanogens and sulfate-reducing bacteria) to degrade complex organic compounds during the reaction. Through organic matter fermentation, *Synergistota* produce formate and H_2, which can be utilized by methanogens to generate CH_4, thereby facilitating interspecies hydrogen transfer and electron transfer among microorganisms (Qiu *et al.* 2024). After the addition of modified biochar, the abundance of *Synergistota* significantly increased from 2.9% to 9.1%, indicating that the excellent electrochemical activity of

biochar enhanced interspecies electron transfer, thereby improving methanogenic efficiency. *Chloroflexota* mainly participate in cellulose and hemicellulose hydrolysis and the acidogenesis process (Nie *et al.* 2025). Additionally, they form syntrophic relationships with methanogens and are more active under high-temperature or low H_2 partial pressure conditions. Compared with the control phase, the relative abundance of *Chloroflexota* increased from 2.2% to 7.6% after the addition of modified biochar, indicating that the system maintained a favorable H_2 consumption rate and methanogenic performance.

It is important to interpret phylum-level community changes with caution, as phyla such as *Bacillota* encompass microorganisms with diverse and even contrasting metabolic capabilities. For instance, while some *Bacillota* members (*e.g.*, *Clostridium spp*.) are key fermentative bacteria involved in hydrogen and volatile fatty acid production, others may participate in syntrophic acetate oxidation or even methanogenesis-related processes. In our CO_2 biomethanation system, which is continuously supplied with H_2/CO_2 rather than complex organic polymers, the functional relevance of phylum-level shifts must be corroborated by genus- or species-level analysis.

Figure 7 (b) shows the relative abundances of bacterial communities at the genus level across different stages. Compared with the control phase, the addition of modified biochar slightly altered the relative abundances of microbial groups, such as *norank_o__Bacteroidales* and *norank_o__MBA03*, but remained highly abundant. *DMER64*, a genus known to participate in syntrophic interactions with methanogens through the exchange of H_2 or formate (*i.e.*, interspecies hydrogen transfer, IHT), increased in relative abundance from 4.3% to 6.1% (Hu *et al.* 2023). The relative abundance of *Thermovirga*, a key functional microorganism in microbial electrolysis cells for enhancing anaerobic digestion, increased from 1.8% to 6.0% (Nie *et al.* 2025). The observed enrichment of electroactive taxa and the sustained VFA degradation under high H_2 partial pressure are consistent with the hypothesis that the modified biochar may have facilitated DIET. Nevertheless, we acknowledge that direct evidence (*e.g.*, biochar conductivity measurements, electrochemical characterization, or metatranscriptomic analysis of DIET-related genes) is needed to confirm this mechanism. Therefore, DIET should be considered a plausible contributing pathway rather than a definitively proven mechanism in the present study.

Microbial samples were collected at two time points per phase, which helps distinguish temporal drift from treatment effects. Samples were taken on days 24 and 51 (control phase) and days 79 and 102 (biochar phase). If the observed community shifts were purely due to temporal drift, one would expect a gradual, unidirectional change across all four time points. Instead, the communities within each phase showed greater similarity to each other than to communities in the other phase—the enrichment of *Synergistota*, *Chloroflexota*, and *Methanothrix* was consistent at both biochar-phase time points (D79 and D102) and differed from both control-phase time points (D24 and D51). This pattern suggests that the biochar addition was the primary driver of the shift, rather than a random temporal trend.

Archaeal community analysis

Figure 7 (a) shows the relative abundances of archaeal communities at the phylum level across different stages. The main phyla identified included Methanobacteriota, Halobacteriota, Thermoproteota, Aenigmarchaeota, and Thermoplasmatota. *Methano-bacteriota*, a dominant archaeal phylum in both anaerobic digestion and CO_2 biomethanation systems, can convert acetate, H_2, CO_2, and methylated small molecules

into CH_4 (Huang *et al.* 2024). It remained the dominant archaeal phylum both before and after the addition of modified biochar, and its relative abundances in the four samples were 84.2, 76.6, 81.2, and 75.7%. Some strains within *Halobacteriota*, including *Halanaerobium*, are involved in the metabolism of proteins and carbohydrates, facilitating the production of acetate, H_2, and CO_2 (Ji *et al.* 2024). Due to the relatively low organic matter concentration in the CO_2 biomethanation system, the abundance of *Halobacteriota* remained low and slightly changed. *Thermoproteota* includes several extremely thermophilic groups, such as *Pyrobaculum*, that decompose peptides and sugars. Kohtz *et al.* used stable isotope tracing, genomic, and transcriptomic analyses to demonstrate that *Methanomethylicia* grows through methyl-reducing hydrogenotrophic methanogenesis and plays an important role in the carbon cycle (Kohtz *et al.* 2024).

It is important to note that while phylum-level classification, such as the detection of *Halobacteriota* and *Thermoproteota*, may suggest the presence of organisms with atypical metabolisms (*e.g.*, halophilic or thermophilic), their low relative abundance and the limitations of 16S rRNA gene-based taxonomy imply that these sequences likely represent either 'passenger' DNA from the feedstock, uncultured lineages with yet-unresolved ecophysiologies, or annotation artifacts.

Figure 7 (b) presents the relative abundances of archaeal communities at the genus level across stages, with *Methanobacterium*, *Methanothrix*, *norank_c__Bathyarchaeia*, *Candidatus_Methanofastidiosum*, and *Methanobrevibacter* showing relatively high abundances. *Methanobacterium*, *Candidatus_Methanofastidiosum*, and *Methanospirillum* are hydrogenotrophic methanogens. *Methanobacterium* converts H_2 and CO_2 into CH_4, whereas *Candidatus_Methanofastidiosum* requires additional methyl compounds for methanogenesis. Some studies have shown that *Methanobacterium* can produce CH_4 by accepting electrons through DIET (Lin *et al.* 2018). After the addition of modified biochar, the relative abundance of *Methanobacterium* in the four samples was 80.3, 75.4, 78.1, and 70.0%, remaining the dominant genus in the system. However, the effect of biochar on DIET and related microorganisms requires further investigation. *Methanothrix* is an acetoclastic methanogen that produces CH_4 through the acetate cleavage pathway. Some studies have also shown that *Methanothrix* can produce CH_4 through DIET interactions with iron-reducing bacteria (Jin *et al.* 2024). Compared with the control phase, the relative abundance of *Methanothrix* increased from 7.9% to 12.6% after the addition of modified biochar, possibly due to the enhanced conductivity of the modified biochar. The enrichment of acetoclastic methanogens by modified biochar may be a key biological factor contributing to the improved organic matter degradation rate.

Methanosarcina and *Methanomassiliicoccus* are both mixotrophic methanogens (Chen *et al.* 2024). *Methanosarcina* can utilize H_2, CO_2, acetate, methanol, and other substrates for methanogenesis and can adapt to high organic loading conditions. In contrast, *Methanomassiliicoccus* is the predominant methanogen group in the rumen of ruminants. After the addition of modified biochar, the relative abundance of *Methanomassiliicoccus* increased from 0.15% to 0.53%, whereas that of *Methanosarcina* decreased from 0.34% to 0.05%. In addition, *norank_c__Bathyarchaeia* is a non-methanogenic archaeal group involved in the degradation of proteins and fatty acids and maintains syntrophic relationships with methanogens. Compared with the control phase, the relative abundance of *norank_c__Bathyarchaeia* increased from 9.5% to 14.2%, indicating that the addition of modified biochar may promote the degradation of organic matter and VFAs in the system.

CONCLUSIONS

1. This study systematically investigated the synergistic effects of trace element-loaded biochar on CO_2 biomethanation, providing both mechanistic insights and process optimization strategies.
2. Among the biochars tested, cattle manure biochar pyrolyzed at 400 °C (CM400, without trace element loading) exhibited the highest methanogenic enhancement, increasing cumulative methane yield 12.1% compared to the control.
3. Response surface methodology identified an optimal trace element mixture (Fe: 15.1 $mg \cdot L^{-1}$, Co: 1.5 $mg \cdot L^{-1}$, Ni: 0.6 $mg \cdot L^{-1}$). The regression model predicted a predicted maximum cumulative methane yield of 132.7 $mL \cdot gVS^{-1}$, representing a 12.9% improvement over the control.
4. The novel modified biochar, prepared by loading the optimal trace elements onto CM400, increased the volumetric methane production (VMP) 19.8% and raised the hydrogen loading capacity 50% (from 2.0 to 3.0 $L_{H2}/\cdot L_{reactor}^{-1} \cdot d^{-1}$) over the control phase, while concurrently improving organic matter removal and system stability. Overall, this additive showed potential to overcome key abiotic limitations—including poor gas-liquid mass transfer, insufficient pH buffering, volatile fatty acid (VFA) accumulation, and trace element deficiency—as well as biotic limitations such as thermodynamic constraints on interspecies electron transfer, suboptimal enzyme activity, and low microbial community diversity.
5. This strategy offers a practical pathway for integrating biological methanation into multi-energy distributed systems. By coupling surplus renewable electricity (via H_2 production) with CO_2 utilization, the process enables Power-to-Gas energy storage in the form of pipeline-compatible CH_4.

ACKNOWLEDGEMENTS

This work was supported by the National Key Technologies Research and Development Program of China under the project "Research and Development of Key Technologies and Equipment for Novel High-Efficiency Energy and Fertilizer Utilization of Diverse Agricultural Wastes" (Grant No. 2025YFD1700602).

Use of Generative AI

No generative AI tools were used in the writing of this text, the analysis of data, or the compilation of references

REFERENCES CITED

Bardi, M. J., Vinardell, S., Astals, S., and Koch, K. (2023). "Opportunities and challenges of micronutrients supplementation and its bioavailability in anaerobic digestion: A critical review," *Renewable and Sustainable Energy Reviews* 186, article 113689. https://doi.org/10.1016/j.rser.2023.113689

Bu, J., Hu, B.-B., Wu, H.-Z., and Zhu, M.-J. (2022). "Improved methane production with redox-active/conductive biochar amendment by establishing spatial ecological niche and mediating electron transfer," *Bioresource Technology* 351, article 127072. https://doi.org/10.1016/j.biortech.2022.127072

Burkhardt, M., Koschack, T., and Busch, G. (2015). "Biocatalytic methanation of hydrogen and carbon dioxide in an anaerobic three-phase system," *Bioresource Technology* 178, 330-333. https://doi.org/10.1016/j.biortech.2014.08.023

Chen, R., Zhou, X., Huang, L., Ji, X., Chen, Z., and Zhu, J. (2024). "Effects of yeast inoculation methods on caproic acid production and microbial community during anaerobic fermentation of Chinese cabbage waste," *Journal of Environmental Management* 356, article 120632. https://doi.org/10.1016/j.jenvman.2024.120632

Cristiani, L., Leobello, L., Zeppilli, M., and Villano, M. (2023). "Role of C/N ratio in a pilot scale microbial electrolysis cell (MEC) for biomethane production and biogas upgrading," *Renewable Energy* 210, 355-363. https://doi.org/10.1016/j.renene.2023.04.049

Dong, D., Kyung Choi, O., and Woo Lee, J. (2022). "Influence of the continuous addition of zero valent iron (ZVI) and nano-scaled zero valent iron (nZVI) on the anaerobic biomethanation of carbon dioxide," *Chemical Engineering Journal* 430, article 132233. https://doi.org/10.1016/j.cej.2021.132233

Ghofrani-Isfahani, P., Tsapekos, P., Peprah, M., Kougias, P., Zhu, X., Kovalovszki, A., Zervas, A., Zha, X., Jacobsen, C. S., and Angelidaki, I. (2021). "*Ex-situ* biogas upgrading in thermophilic up-flow reactors: The effect of different gas diffusers and gas retention times," *Bioresource Technology* 340, article 125694. https://doi.org/10.1016/j.biortech.2021.125694

Gonçalves, R. F., Bastos, L. P., Nariyoshi, Y. N., Borges, R. M., Keller, R., and Silveira, D. D. (2025). "Assessment of selected parameters in CO_2 and CH_4 mass transfer during photosynthetic biogas upgrading using bubble columns filled with wastewater-derived microalgae," *Energy & Fuels* 39(15), 7314-7325. https://doi.org/10.1021/acs.energyfuels.4c05688

Gong, Y., Guo, X., Huang, P., Guo, Y., Jiang, Y., Jiang, F., Ma, Z., and Ji, S. (2026). "A spatial ZVI strategy boosts digestion performance and ammonium recovery through in-situ conductive mineral formation," *Journal of Water Process Engineering* 82, article 109537. https://doi.org/10.1016/j.jwpe.2026.109537

Greenberg, A. E., Trussell, R. R., Clesceri, L. S., Greenberg, A., American Public Health Association, American Water Works Association, and Water Pollution Control Federation (1985). *Standard Methods for the Examination of Water and Wastewater*, American Public Health Association, Washington, D.C., USA.

Han, X., Tang, J., Miao, X., Zhang, X., and Kong, R. (2025a). "Preparation and permeability evaluation of carbon molecular sieve membrane for efficient separation of H_2 / CH_4 in hydrogen-doped pipeline," *Journal of Physics: Conference Series* 3048(1), article 012159. https://doi.org/10.1088/1742-6596/3048/1/012159

Han, Y., Luo, Y., Zhang, L., Lu, X., Luo, X., Wu, X., and Zan, F. (2025b). "Deciphering the mechanistic insight into modified biochar for distinct anaerobic digestion processes: Surface functional groups and electron-transmitting capabilities," *Journal of Environmental Chemical Engineering* 13(2), article 115581. https://doi.org/10.1016/j.jece.2025.115581

Hu, Y., Wang, X., Zhang, S., Liu, S., Hu, T., Wang, X., Wang, C., Wu, J., Xu, L., Xu, G., *et al.* (2023). "Microbial response behavior to powdered activated carbon in high-

solids anaerobic digestion of kitchen waste: Metabolism and functional prediction analysis," *Journal of Environmental Management* 337, article 117756. https://doi.org/10.1016/j.jenvman.2023.117756

Huang, W., Wang, F., Xia, X., Fang, S., Cheng, X., Zhou, A., Feng, L., Wang, D., and Luo, J. (2024). "Tannic acid modulation of substrate utilization, microbial community, and metabolic traits in sludge anaerobic fermentation for volatile fatty acid promotion," *Environmental Science & Technology* 58(22), 9792-9803. https://doi.org/10.1021/acs.est.3c08678

Ji, X., Chen, Z., Shen, Y., Liu, L., Chen, R., and Zhu, J. (2024). "Hexanoic acid production and microbial community in anaerobic fermentation: Effects of inorganic carbon addition," *Bioresource Technology* 403, article 130881. https://doi.org/10.1016/j.biortech.2024.130881

Jin, B., Jia, Y., Cheng, K., Chu, C., Wang, J., Liu, Y., Du, J., Wang, L., Pang, L., Ji, J., *et al.* (2024). "Facilitating effects of the synergy with zero-valent iron and peroxysulfate on the sludge anaerobic fermentation system: Combined biological enzyme, microbial community and fermentation mechanism assessment," *Chemosphere* 355, article 141805. https://doi.org/10.1016/j.chemosphere.2024.141805

Kalbermatten, C. L., Jordan, S., Pothier, J. F., Nägele, H.-J., Smits, T. H. M., and Merkle, W. (2025). "Performance optimization of a trickle-bed reactor for hydrogenotrophic methane production in a power-to-gas approach," SSRN (Preprint). https://doi.org/10.2139/ssrn.5134738

Kohtz, A. J., Petrosian, N., Krukenberg, V., Jay, Z. J., Pilhofer, M., and Hatzenpichler, R. (2024). "Cultivation and visualization of a methanogen of the phylum Thermoproteota," *Nature* 632(8027), 1118-1123. https://doi.org/10.1038/s41586-024-07631-6

Li, R., Qiu, C., Chen, X., Liu, N., Zhang, Y., Qi, L., and Wang, S. (2026). "Effects of thermal alkaline hydrolysis and biochar addition on anaerobic digestion of sewage sludge and fate of antibiotic resistance genes," *Bioresource Technology* 441, article 133569. https://doi.org/10.1016/j.biortech.2025.133569

Li, Y., and Kobayashi, T. (2025). "Impacts of biochar addition on anaerobic digestion of food waste with hydrogen," *Bioresource Technology* 438, article 133245. https://doi.org/10.1016/j.biortech.2025.133245

Liang, W., Li, G., Dai, Y., Zhou, H., Wang, Y., Han, Y., Qi, Y., Wang, D., Jiang, K., and Zhu, Q. (2026). "Trace element supplementation enables sustainable high-straw dry anaerobic digestion by suppressing acidification and boosting biogas *via* microbial network rewiring," *Sustainability* 18(3), article 1395. https://doi.org/10.3390/su18031395

Lin, R., Cheng, J., Ding, L., and Murphy, J. D. (2018). "Improved efficiency of anaerobic digestion through direct interspecies electron transfer at mesophilic and thermophilic temperature ranges," *Chemical Engineering Journal* 350, 681-691. https://doi.org/10.1016/j.cej.2018.05.173

Méndez-Contreras, J. M., Atenodoro-Alonso, J., López-Escobar, L. A., and Nava-Valente, N. (2024). "Enhanced biogas production from thermophilic anaerobic digestion of poultry slaughterhouse sludge: Effect of thermal pretreatment and micronutrients supplementation," *Waste and Biomass Valorization* 15(4), 2201-2214. https://doi.org/10.1007/s12649-023-02277-3

Moestedt, J., Nordell, E., Shakeri Yekta, S., Lundgren, J., Martí, M., Sundberg, C., Ejlertsson, J., Svensson, B. H., and Björn, A. (2016). "Effects of trace element

addition on process stability during anaerobic co-digestion of OFMSW and slaughterhouse waste," *Waste Management* 47, 11-20. https://doi.org/10.1016/j.wasman.2015.03.007

Nie, E., He, P., Zhang, H., and Lü, F. (2025). "Genome-centric metagenomic analysis unveils the influence of temperature on the microbiome in anaerobic digestion," *Journal of Environmental Sciences* 158, 516-526. https://doi.org/10.1016/j.jes.2024.10.007

Pan, J., Ma, J., Liu, X., Zhai, L., Ouyang, X., and Liu, H. (2019). "Effects of different types of biochar on the anaerobic digestion of chicken manure," *Bioresource Technology* 275, 258-265. https://doi.org/10.1016/j.biortech.2018.12.068

Qiu, W., Liu, Y., Li, S., Fan, G., Pan, C., Song, G., and Cheng, Q. (2024). "Impact of nZVI and nZVI/BC on the anaerobic digestion of piggery wastewater," *Bioremediation Journal* 28(4), 432-442. https://doi.org/10.1080/10889868.2023.2282640

Rachbauer, L., Voitl, G., Bochmann, G., and Fuchs, W. (2016). "Biological biogas upgrading capacity of a hydrogenotrophic community in a trickle-bed reactor," *Applied Energy* 180, 483-490. https://doi.org/10.1016/j.apenergy.2016.07.109

Ramírez-Amador, F., Paul, S., Kumar, A., Lorent, C., Keller, S., Bohn, S., Nguyen, T., Lometto, S., Vlegels, D., Kahnt, J., *et al.* (2025). "Structure of the ATP-driven methyl-coenzyme M reductase activation complex," *Nature* 642(8068), 814-821. https://doi.org/10.1038/s41586-025-08890-7

Šafarič, L., Yekta, S. S., Svensson, B. H., Schnürer, A., Bastviken, D., and Björn, A. (2020). "Effect of cobalt, nickel, and selenium/tungsten deficiency on mesophilic anaerobic digestion of chemically defined soluble organic compounds," *Microorganisms* 8(4), article 598. https://doi.org/10.3390/microorganisms8040598

Santamaría, D., Sánchez, A., and Martín, M. (2025). "Scaling down analysis of e-methane production: Advancing towards distributed manufacturing," *Renewable Energy* 245, article 122792. https://doi.org/10.1016/j.renene.2025.122792

Salazar-Batres, K. J., and Moreno-Andrade, I. (2025). "Review of the effects of trace metal concentrations on the anaerobic digestion of organic solid waste," *BioEnergy Research* 18(1), article 24. https://doi.org/10.1007/s12155-025-10826-y

Shin, D. (2025). "Effect of trace elements on mesophilic anaerobic digestion of food wastewater and optimization of biogas production," *Environmental Science and Pollution Research* 32(30), 18014-18024. https://doi.org/10.1007/s11356-025-36693-w

Suanon, F., Sun, Q., Mama, D., Li, J., Dimon, B., and Yu, C.-P. (2016). "Effect of nanoscale zero-valent iron and magnetite (Fe_3O_4) on the fate of metals during anaerobic digestion of sludge," *Water Research* 88, 897-903. https://doi.org/10.1016/j.watres.2015.11.014

Wang, F., Li, Y., Zhang, L., Su, Y., Zhang, Y., Hong, S., Zhan, M., and Xie, B. (2025). "Biochar alleviates adverse effects of polystyrene microplastics on anaerobic digestion performance of food waste and antibiotic resistance gene propagation," *Bioresource Technology* 434, article 132771. https://doi.org/10.1016/j.biortech.2025.132771

Wang, N., Yang, W., Qu, Y., Chen, Q., Xiong, T., Wang, X., Ko, J. H., and Xu, Q. (2026). "Mechanistic insights into the spontaneous failure-to-success transition in pilot-scale anaerobic digestion of food waste: Roles of volatile fatty acids and microbial community dynamics," *Environmental Research* 300, article 124418. https://doi.org/10.1016/j.envres.2026.124418

Wu, L., Hou, Z., Zhang, L., and Lüddeke, T. C. (2025). "A simulation study of biogeochemical interactions in cyclic underground bio-methanation of carbon dioxide and hydrogen," *Petroleum Exploration and Development* 52(4), 1102-1112. https://doi.org/10.1016/S1876-3804(25)60626-4

Xirostylidou, A., Gaspari, M., Kontogiannopoulos, K. N., Ghiotto, G., Treu, L., Campanaro, S., Zouboulis, A. I., and Kougias, P. G. (2024). "Biomethanation on demand: Continuous and intermittent hydrogen supply on biological CO_2 methanation," *Chemical Engineering Journal* 495, article 153677. https://doi.org/10.1016/j.cej.2024.153677

Ye, Q., Fang, H., Tang, R., Li, M., and Li, X. (2026). "Synergistic parameter optimization unlocks high-efficiency H_2/CO_2 bio-methanation: Decoupling mass transfer enhancement from microbial trade-offs," *Bioresource Technology* 450, article 134459. https://doi.org/10.1016/j.biortech.2026.134459

Yuan, H.-Y., Ding, L.-J., Zama, E. F., Liu, P.-P., Hozzein, W. N., and Zhu, Y.-G. (2018). "Biochar modulates methanogenesis through electron syntrophy of microorganisms with ethanol as a substrate," *Environmental Science & Technology* 52(21), 12198-12207. https://doi.org/10.1021/acs.est.8b04121

Zhao, Z., Wu, H., An, Y., Huang, L., and Zhang, G. (2025). "Enhancing anaerobic digestion of waste activated sludge with iron modified tea-based biochar *via* improving electron transfer and metabolic activity," *Renewable Energy* 242, article 122458. https://doi.org/10.1016/j.renene.2025.122458

Zheng, X., Liu, S., Faisal, S., Khan, A., Danish, M. I., Rehman, A., and Du, D. (2025). "Enhanced biomethane conversion and microbial community shift using anaerobic/mesophilic co-digestion of dragon fruit peel and chicken manure," *Biology* 15(1), article 83. https://doi.org/10.3390/biology15010083

Zhou, G., Huang, X., Zhang, S., Xiang, Z., Wei, J., Ma, S., Teng, X., and Zheng, Z. (2024). "Volatile fatty acids (VFAs) production from sludge and chicken manure anaerobic co-fermentation: Effects of mixing ratio and microbial mechanisms," *Journal of Environmental Chemical Engineering* 12(5), article 114014. https://doi.org/10.1016/j.jece.2024.114014

Zhu, X., Zhang, Y., Yellezuome, D., Wang, Z., Liu, X., and Liu, R. (2024). "The effects of co-supplemented Fe, Co and Ni on Fe bioavailability and microbial community structure in mesophilic food waste anaerobic digestion by using response surface methodology," *Renewable Energy* 229, article 120776. https://doi.org/10.1016/j.renene.2024.120776

Article submitted: June 23, 2026; Peer review completed: August 1, 2026; Revised version received and accepted: August 10, 2026; Published: August 26, 2026.
DOI: 10.15376/biores.21.4.10070-10097

APPENDIX

Supplementary Material

Table S1. Experimental Coding Table

Trace element		Code	
	-1	0	1
Fe (mg·L^{-1})	10	15	20
Co (mg·L^{-1})	1.0	1.5	2.0
Ni (mg·L^{-1})	0.1	0.55	1.0

Table S2. Experimental Design and Results of Gas Production

No.	Trace Element (mg·L^{-1})			Cumulative Methane Yield (mL·gVS^{-1})
	Fe	Co	Ni	
0	0	0	0	120.336
1	20	1.5	1.0	121.859
2	10	1.5	0.1	118.935
3	15	1.5	0.55	134.873
4	15	1.0	0.1	116.515
5	20	1.5	0.1	120.296
6	15	2.0	0.1	116.897
7	10	2.0	0.55	115.597
8	15	1.5	0.55	131.074
9	20	2.0	0.55	116.483
10	15	1.0	1.0	117.594
11	10	1.0	0.55	112.623
12	10	1.5	1.0	121.698
13	20	1.0	0.55	113.439
14	15	1.5	0.55	131.998
15	15	2.0	1.0	118.144
16	15	1.5	0.55	130.292
17	15	1.5	0.55	134.824

Table S3. Experimental Full-mode ANOVA

Source of Variation	Sum of Squares	Degrees of Freedom	Mean Square	F value	P value	Significance
Model	894.78	9	99.42	31.83	< 0.0001	**
A-Fe	1.30	1	1.30	0.4159	0.5395	
B-Co	6.04	1	6.04	1.93	0.2071	
C-Ni	5.53	1	5.53	1.77	0.2250	
AB	0.0012	1	0.0012	0.0004	0.9848	
AC	0.3600	1	0.3600	0.1152	0.7442	
BC	0.0071	1	0.0071	0.0023	0.9634	
A^2	226.45	1	226.45	72.49	< 0.001	
B^2	485.95	1	485.95	155.56	< 0.004	
C^2	88.38	1	88.38	28.29	0.0011	
Residual	21.87	7	3.12			
Lack of fit	3.74	3	1.25	0.2749	0.8415	Not significant
Pure error	18.13	4	4.53			
Total error	916.65	16				
	R^2 = 0.9761		R^2_{Adj} = 0.9455		CV = 1.45	

Note: *: significant difference (P < 0.05)